Local properties in rapidity in the multiperipheral picture

N. Murai*
Department of Physics, Westfield College, University of London, Kidderpore Avenue, London NW3 7ST, England
(Received 19 February 1976)

By making statistical assumptions, we attempt to extend the kinematical domain beyond the strong-ordering limit in the multiperipheral picture. The relaxation of the strong-ordering hypothesis leads to an apparent clustering among final particles. An attractive component of short range in rapidity is found in two-particle correlations at fixed multiplicity and in the distribution of gap lengths between adjacent secondaries. In addition, we remark upon the qualitative consistency of our model with the average track number per zone associated with local compensation of charge.

I. INTRODUCTION

The cluster model has recently become one of the most popular phenomenological tools for dealing with multiparticle production data.[1,2] Neutral-cluster models with the independent-emission picture have enjoyed some success in reproducing the local properties in rapidity of the processes. It is usually assumed that the mobility of secondaries is about one unit of rapidity[3,4] from the clusters. However, as far as one persists with the current parametrization, the neutrality of the clusters has been almost ruled out[5,6] by the observed distribution of rapidity gap lengths between particles adjacent in rapidity, when the gaps are labeled by the amount of charge transferred across them. This observation raises the question as to whether the clustering is merely a convenient language, or whether real clusters are actually produced. The aim of this article is to suggest the former possibility.

In this article we shall be concerned mainly with two observable quantities:

(a) two-particle correlations at fixed multiplicity, in Sec. III, and

(b) rapidity-gap distribution in pp collisions, in Sec. IV.

Comparison with experiment will remain tentative, but it will be shown that there is a rough correspondence between our calculated values and those measured so far.

In Sec. II we shall present a model with secondaries produced directly which is based on the multiperipheral picture.[7] The multiperipheral model (MPM) has been the prototype for a short-range correlation mechanism. However, the simplified MPM of Chew and Pignotti[8,9] (the two-channel model by Snider[10] will be referred to in Sec. V) cannot reproduce the attractive short-range component mentioned in (a) (see Refs. 11 and 12) and (b). This version of the MPM makes use of the strong-ordering hypothesis[13] that the particle's ordering in rapidity is their ordering along the multiperipheral chain. Indeed, this hypothesis should work well in evaluating single-particle distributions and in investigations at large rapidity gap (more than one unit of rapidity). However, it is doubtful that it holds for small rapidity separation between emitted particles, which is important for clustering phenomena. In the strong-ordering limit the subenergies given to the multiperipheral links are large and, therefore, so are the rapidity separations. Moreover, we can exploit empirical mean values[14] of track numbers per zone associated with local compensation of charge[15] in order to exclude the strong-ordering hypothesis in the literal sense.

Thus an issue of central concern will be how to extend our kinematical domain from the strong-ordering limit. We shall assume that the asymptotic Regge form is valid, in an average sense, in the low-subenergy resonance region of a partial multiperipheral chain. Furthermore, outside the small-momentum-transfer region, the probability function (cross section) associated with a portion of the chain will be small at high subenergies. However, it will not be zero. We shall interpret it as the tail of the forward scattering in an average sense.

It would be difficult to make a completely dynamical consideration on the above situation. Therefore, we treat it in a statistical way. Our considerations are expressed in the following two assumptions: (1) The probability that a particle is emitted at a given rapidity point is uniform, if there are no subsidiary conditions. One will see that this assumption is consistent with the MPM. In the large-rapidity-gap region, our model exhibits the strong-ordering limit. Therefore, the probability can be related to the intercept of Regge trajectories exchanged.[10,16] In this sense, our model is a natural generalization of a one-channel MPM with strong ordering. (2) Secondly, we adopt

the notion of limited charge exchange (LCEX)[6,17,18] between final particles. That is to say, exotic-charge exchanges are forbidden. Indeed, this concept is an immediate abstraction from the exchange picture.

At first glance, it seems to be pointless to investigate clustering phenomena at small rapidity separation through the exchange picture, which is obtained in the strong-ordering limit. We shall find the justification in the central-limit theorem and show that the asymptotic Regge behavior is important for results which are valid in the small-gap region.

The conclusions will be given in Sec. V, where we shall discuss the relationship of our model to other current ones.

II. THE MODEL

This section is divided into four parts: Before illustrating our model in detail, we describe the basic framework in Sec. II A. Section II B deals with rapidity distribution and Sec. II C with quantum-number distribution. Finally, particle distributions will be given in Sec. II D.

A. Basic Framework

All theoretical quantities will be calculated at *fixed multiplicity*. We shall temporarily regard inclusive quantities as semiempirical through the use of observed multiplicity distributions. The basic framework is made up of the following points:

(P1) Our basic assumption is that those quantities at large fixed multiplicity are dominated by the short-range component of two-particle correlations, which is generated by an exchange mechanism. An advantage of these quantities has already been pointed out by Berger.[19]

(P2) If we can restrict ourselves to multiplicities larger than $\frac{1}{2}$ the mean multiplicity, it is possible to ignore diffractive effects. Whether intrinsic long-range correlations[20] are present within the nondiffractive component is uncertain. However, we assume (P1).

(P3) We do not take account of energy-momentum-conservation constraints. This is discussed in Ref. 21 for two-particle correlations, in Refs. 22 and 23 for rapidity-gap distributions, and in Refs. 9 and 24 for single-particle distributions. We shall briefly discuss the constraints in Secs. III and IV.

The following assumption is related to (P3):

(P3′) The maximum rapidity Y of pions is large: $Y \gg 1$.

(P4) Mediating resonance production[7,18,25] is neglected.

Experimentally, this occupies a large fraction (about 30% in pp collisions) of the final-meson cross sections.[26] Assuming (P3) and (P4) would be a considerable idealization. However, at the present stage, which is not the ultimate one, including these effects reduces our insight into genuine results from the relaxation of strong ordering.

(P5) Owing to the small average value of transverse momenta of secondaries, we consider only rapidity dependence. A brief comment will be made in Sec. V.

(P6) We may either treat production amplitudes or probability functions (differential cross sections). We choose the latter for simplicity, although we are not strictly justified in this choice.[27] This corresponds, in some sense, to the ladder approximation of the MPM.

(P7) We take the so-called leading-particle effect into account: Two protons are produced at both ends of a multiperipheral chain.

(P8) Except for the two protons, only pions are produced. This is justified by the dominance of pion production even at CERN ISR energies.[28]

Expressing explicitly the LCEX mentioned as assumption (2) in Sec. I, we make a rather restrictive assumption:

(P9) Only charges $+1$, 0, -1 are exchanged.

We usually invoke the strong-ordering hypothesis (abbreviated as SOH in this subsection) to simplify the MPM. However, assuming both (P9) and SOH contradicts experimental analyses[14] of local compensation of charge.[15] That is to say, (P9) and SOH imply that the mean number of charges $\langle n_z \rangle$ per zone is equal to 2 irrespective of charge multiplicity n_c. (Throughout this section, leading protons are excluded in obtaining $\langle n_z \rangle$.) By contrast, the observed $\langle n_z \rangle$ increases with n_c. Their values are rather near (somewhat smaller) to those of a set of fictitious events obtained by randomly reassigning charges to the observed tracks.[14] It is concluded in Ref. 14 that the difference between the data and those of the randomized-charge model is meaningful. Furthermore, the leading-proton effect (P7) cannot explain the discrepancy, although this effect does reduce it appreciably.

To understand the above observation clearly, in Table I we compare the data in the central region with $\langle n_z \rangle$ calculated in a simple random-production picture: Positive and negative charges are emitted with the same weight under total charge conservation.

Table I implies that the actual situation lies between the two extreme cases: the MPM with (P9) and SOH, and the random-production picture. It is natural to relax SOH in constructing our model, since (P9) is more deeply connected to multiperipheral dynamics. Indeed, the hypothesis of

TABLE I. Average number of charged particles per zone in the central region. This is plotted versus charge multiplicity. The observed values (Ref. 12) are compared with those of a random-production picture given in the text.

n_c	102 GeV/c	400 GeV/c	$\langle n_Z \rangle$ (random)
4	2.00 ± 0.01	2.00 ± 0.01	2.0
6	2.28 ± 0.03	2.21 ± 0.03	2.2
8	2.52 ± 0.03	2.46 ± 0.03	2.72
10	2.72 ± 0.03	2.59 ± 0.05	3.03

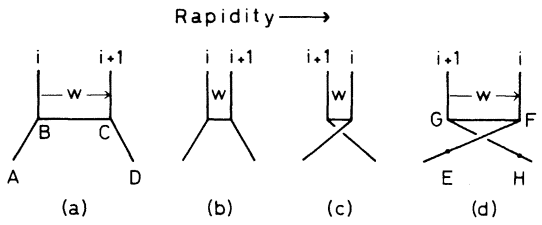

FIG. 1. Various types of multiperipheral subchain including the pions i and $i+1$. AB, BC, CD, etc. are Reggeon lines.

LCEX is precisely the content of the local-charge-compensation postulate.

B. Rapidity distribution

Our relaxation of the strong-ordering hypothesis is intuitive and statistical. The fundamental assumption is

(P10) The probability that a particle is emitted with rapidity between y and $y+dy$ is proportional to dy, if no subsidiary condition is imposed. The constant of proportionality, D, is uniform throughout the whole rapidity range. This assumption would lead to the central plateau of inclusive spectra in the high-energy limit. Suppose that a particle is produced at a certain rapidity. The probability of finding a gap r around it, i.e., the nearest particle is rapidity space at distance r, is[29]

$$p(r) = \tfrac{1}{2} D e^{-Dr} , \tag{2.1}$$

where $p(r)$ is normalized to unity when integrated over r in the infinite rapidity space. Snider[10] showed that (2.1) is consistent with the MPM in the strong-ordering limit and that D is related to the intercept $\alpha(0)$ of the Regge trajectory exchanged in the following way[10,16]:

$$D = 2 - 2\alpha(0) . \tag{2.2}$$

We require (2.1) with (2.2) for an outgoing pair, to neighbors on the multiperipheral chain, but not necessarily to be adjacent in rapidity. Equation (2.1) holds in any one-dimensional space. Here, the space is the multiperipheral chain with rapidity as metric. The above trick does not contradict the derivation of (2.2), since our model almost coincides with the MPM with strong ordering in the large-gap region (see Sec. IV).

It is well known from two-body reactions that the ordinary Regge trajectories, the highest ones in the Chew-Frautschi plot, have the intercept $\alpha(0) \approx \frac{1}{2}$. With the choice of $\alpha(0) = 0.53$,[30] one obtains $D = 0.94$ by (2.2).

A final simplification is the following:

(P11) The emission probability of a particle is proportional to that of its nearest neighbors in the multiperipheral chain, but independent of other particles.

Under assumption (P11), if a particle is emitted with rapidity y, then the probability that a secondary particle separated from it by k links of the multiperipheral chain is produced with rapidity $y+\Delta y$ is

$$F_k(\Delta y) = \overbrace{p \otimes \cdots \otimes p}^{k}(\Delta y) , \tag{2.3}$$

where $\otimes$ means convolution. By using the Fourier transform, (2.3) leads to

$$F_k(\Delta y) = \frac{D\sqrt{\pi}}{\Gamma(k)} \left(\frac{D\Delta y}{2}\right)^{k-1/2} K_{k-1/2}(D\Delta y) , \tag{2.4}$$

where $K_j(x)$ is a modified Bessel function of the second kind.[31]

Now for convenience in the subsequent discussion we give some notations which will be employed throughout the present article. At fixed multiplicity N we assign the numbers $1, \ldots, n$ $(N = n+2)$ to pions from left to right along the multiperipheral chain, and denote their rapidities by $y_1, \ldots, y_n$ in the center-of-mass system (c.m.s.) The pion 1 is an immediate neighbor of a proton produced near the "left" kinematical boundary with negative rapidity in the c.m.s. The pion n is connected directly to the other proton.

Let us examine how the strong-ordering hypothesis has been relaxed. Figure 1 shows a portion of multiperipheral graphs contributing to $F_k(\Delta y)$. We denote by s_i the subenergy supplied to the outgoing neighboring pions i and $i+1$. It is expressed as[32]

$$s_i \sim \mu^2 e^w , \tag{2.5}$$

if $w = |y_{i+1} - y_i| \gg 1$, where μ is the longitudinal mass of the pions. Hence, high-subenergy "scattering" is depicted by the graph 1(a) and low-subenergy scattering by the graph 1(b). The form (2.1) means that the low-energy behavior is described by extrapolation from the asymptotic Regge form. Then, from the viewpoint of reso-

nance fluctuation,[33,34] resonance production is not considered [(P4)].

The probability function of the graph 1(d) [or 1(c)] is

$$\frac{D}{2}\, e^{-3Dr} \tag{2.6}$$

since each of the propagations along EF, FG, and GH gives e^{-Dr}. It is seen from (2.6) and (2.1) that the low-energy graph 1(c), not strongly ordered, makes a somewhat smaller, but nearly the same, contribution to F_k as the graph 1(b), while the high-energy contribution of 1(d) is substantially suppressed. More generally, consider n particles outgoing at certain fixed rapidities. One can draw many multiperipheral graphs according to various choices in combining particles with links (Regge trajectories exchanged). It is immediately clear from (2.1) that a particular graph occurs with the probability

$$\left(\frac{D}{2}\right)^n e^{-DS} \tag{2.7}$$

where S is the total length of the multiperipheral chain in rapidity: $S=\sum_{i=1}^{n-1}|y_i - y_{i+1}|$. Hence the highest weight occurs for a graph having the shortest chain length—a strongly ordered graph.

Strictly speaking, we have only exactly forward and backward "scattering" because we are ignoring the transverse momenta [(P5)]. If we refer to 1(a) as forward "scattering," we may think of 1(d) as backward "scattering," regarding the Reggeon lines $EGHF$ as a "black box" describing the scattering. Since the same quantum number is exchanged in the graph 1(d) as in 1(a), the cross section of the former may be the *tail* of that of 1(a). This interpretation is possible in an average sense. The average subenergy $\langle s_i\rangle$ is given by[32]

$$\langle s_i\rangle \lesssim \tau^{1-1/N} s^{1/N}\,, \tag{2.8}$$

where τ is some peripheral range of momentum transfer and s is c.m.s. energy squared. By taking $\tau \approx 1$ (GeV/c)^2 (the inverse of the slope of Regge trajectories), at 205 GeV/c,[35]

$$\langle s_i\rangle \lesssim 1.8 \text{ GeV}^2\,, \tag{2.9}$$

when the total average multiplicity $N=1.5\,(\langle n_c\rangle - 2)+2$ with the charge multiplicity $\langle n_c\rangle$.[36] In the backward direction, (2.9) leads to $t_i \gtrsim -1.8$ GeV/c. The effective Regge trajectory at t_i is $\alpha(t_i) \gtrsim -0.96$ by assuming $\alpha(t)=0.53+0.83t$.[30] The effective slope D_{eff} in the form (2.1) is evaluated by (2.2):

$$D_{\text{eff}} \lesssim 3.9\,, \tag{2.10}$$

which is in fair agreement with

$$3D = 2.8 \tag{2.11}$$

in (2.6). If we employ the usual value $\langle s_i\rangle \sim 1$ GeV^2,[32] the agreement is more complete. We overestimate the probability function when $s_i > \langle s_i\rangle$ and undervalue it when $s_i < \langle s_i\rangle$. It would be, however, plausible to say that, in an average sense, the "scattering" 1(d) is the tail of the forward one in the strong-ordering limit.[37]

By virtue of the central-limit theorem,[38] $F_k(\Delta y)$ can be approximated for large k by

$$F_k(\Delta y) = \frac{D}{(4\pi k)^{1/2}} \exp\left[-\frac{(D\Delta y)^2}{4k}\right]. \tag{2.12}$$

In addition to its simplicity, (2.12) has other advantages over (2.4): Even if (2.1) deviates from the Regge behavior in the small-r region, only the asymptotic form is important for the validity of (2.12). Moreover, the theorem justifies applying (2.12) to small rapidity separations, since (2.12) holds in the region $|\Delta y| < 2(\ln k)^2$.[38] As remarked in Sec. I, this is an important point in our scheme. However, we still ignore resonance production for small k [(P4)].

For future convenience, we define the *direction* of a link: If the rapidity order of two particles connected by the link coincides with their order in the multiperipheral chain, the direction of the link is positive. Otherwise, the direction is negative. In a strongly ordered graph, all links point in the positive direction. Of course, the whole assignment is reversible.

C. Quantum-number distribution

We deal with only the charge on account of assumption (P8). A more general case has been discussed in Ref. 18.

For simplicity, we assume that a kind of trajectory is exchanged between the emitted pions. Hence there is a factorization of the rapidity distribution from the quantum-number part.

Imagine that a link of the multiperipheral chain is one of several charge states with a corresponding probability. The probability for a charge state changes with the links from left to right (or right to left) along the chain. Such a simplification reminds us of probability process, whose discrete time corresponds to the production steps along the chain. We employ Dirac's bra-ket notation $\langle\alpha|$ or $|a\rangle$ to denote an orthonormal charge state with charge α. Let us introduce an operator T, whose matrix element $\langle\beta|T|\alpha\rangle$ represents a transition *probability* from $|\alpha\rangle$ on a link to $|\beta\rangle$ on the nearest-neighbor link, [remember (P6) and apply (P11) also to quantum-number distribution]. Then, $\langle\beta|T^k|\alpha\rangle$ is the probability that $|\alpha\rangle$ transits to $|\beta\rangle$ through "successive" production along k links.[39]

(P12) We impose stochastic conditions on T:

$$\sum_{\alpha} \langle \beta | T | \alpha \rangle = 1, \tag{2.13}$$

$$\sum_{\beta} \langle \beta | T | \alpha \rangle = 1. \tag{2.14}$$

Conservation of probability asserts (2.13). In high-multiplicity events we expect $\pi^{\pm}$, π^0 to be emitted in the central region with the same weight. Charge states in the central region are controlled by T^k ($k \gg 1$). The conditions (2.13) and (2.14) ensure that all charge states occur with equal frequency as $k \to \infty$. (Here we deal with the nonperiodic and irreducible 3×3 matrix T.)

Requirements (P9) and (P12) determine the form of T:

$$T = \begin{array}{c} \begin{matrix} +1 & 0 & -1 \end{matrix} \\ \begin{bmatrix} 1-a & a & 0 \\ a & 1-2a & a \\ 0 & a & 1-a \end{bmatrix} \end{array} \begin{matrix} \\ +1 \\ 0 \\ -1 \end{matrix} \tag{2.15}$$

where $0 < a \leq \frac{1}{2}$. Furthermore, we require that the charge states of $T^k|0\rangle$ approach the large-k limit in the most rapid way possible as k increases. This will be related to a simplification of the quantum-number part of particle distribution (Sec. IV D). It is clear that the smaller the ratio of the second largest to largest eigenvalues of T is, i.e., $1-a:1$, the faster the rate of the approach. Thus, $a = \frac{1}{2}$ gives the most rapid approach.

D. Particle distributions

Combining Secs. II A–II C enables us to obtain pion distribution at the fixed multiplicity N.

We assume that $D = 0$ for the end links to determine the probability of the emission of pion 1, once the "left" proton is produced (P7). Hence we have a uniform distribution. This corresponds to the statistically large end gaps observed.[40] Another reason for this prescription is that we need not take account of empirical proton distribution to obtain analytical expressions for the quantities considered in this paper [(a) and (b) in Sec. I]: The pion 1 does not depend on the location of the proton. In order to make clear that the first pion is associated with the "left" proton, we adopt a somewhat arbitrary cutoff: $y_1 < 0$. A similar consideration applies to pion n.

By virtue of (2.12) [or (2.4)], it is now straightforward to write down the rapidity distribution of the pion i when n pions are produced,

$$\bar{W}_i^n(y_i) = N_R \int_{-Y}^{0} dy_1 \int_0^Y dy_n F_{i-1}(|y_1 - y_i|) \times F_{n-i}(|y_i - y_n|), \tag{2.16}$$

where Y is the maximum rapidity of pions in the c.m.s.,

$$N_R = \frac{1}{\int_{-Y}^{Y} dy_i \int_{-Y}^{0} dy_1 \int_0^Y dy_n F_{i-1}(|y_1 - y_i|) F_{n-i}(|y_i - y_n|)}, \tag{2.17}$$

and

$$F_0(x) = \delta(x). \tag{2.18}$$

The normalization factor N_R is independent of i at very high energy (P3′).

The charge γ of the pion i is distributed as

$$Q_{i,\gamma}^n = \sum_{\alpha,\beta} \frac{\langle 0 | T^{n-i} | \beta \rangle \langle \beta | T_\gamma | \alpha \rangle \langle \alpha | T^{i-1} | 0 \rangle}{\langle 0 | T^n | 0 \rangle}, \tag{2.19}$$

where

$$\langle \beta | T_\gamma | \alpha \rangle = \begin{cases} \langle \beta | T | \alpha \rangle, & \text{if the process } \alpha + \beta + \gamma \text{ is allowed} \\ 0, & \text{otherwise.} \end{cases} \tag{2.20}$$

If $|y_1| > \epsilon$ ($\epsilon \lesssim 0.5$), the results are insensitive to ϵ. One can see in (2.19) that T can be multiplied by an arbitrary constant. Only relative ratios among the components are important. The constant should correspond to the square of a coupling constant.

Finally, we can derive the following expression for the single-pion distribution with charge γ:

$$\rho_N(y, \gamma) \equiv \frac{1}{\sigma_{N,\gamma}} \frac{d\sigma_{N,\gamma}}{dy} = \sum_{i=1}^{n} \bar{W}_i^n(y) Q_{i\gamma}^n, \tag{2.21}$$

where $\sigma_{N,\gamma}$ is the partial cross section for π^γ. It is easy to verify the identity

$$\sum_{\gamma} \int \rho_N(y, \gamma) dy = n. \tag{2.22}$$

Strictly speaking, (2.16) is correct only in the high-energy limit. The pions stray out beyond the kinematical boundary at finite energy. To eliminate this undesirable behavior, one can adopt the well-known technique of reflection in boundary-value problems.[41] One may prefer absorptive boundary conditions to reflective ones to impose $\rho_N(\pm Y, \gamma) = 0$. This consideration requires an infinite series of similar terms to (2.16). It would be inappropriate to go into such detail since we have ignored kinematical constraints, (P3). Instead, a somewhat arbitrary prescription will be made to save computation time[42]: We employ the maximum rapidity of the protons Y_p as Y to suppress pions lost beyond the exact maximum rapidity Y_π of the pions. The apparent exudation of pions beyond Y_p should correspond to the tail of the empirical pion spectrum.

At finite energy, (2.19) is not very satisfactory, since the pions 1 and n are either π^+ or π^- and never π^0. Therefore π^0 production would be a little suppressed, especially at low multiplicity. To remedy this, one should replace T by

$$T_E = \begin{pmatrix} 0 & \frac{1}{3} & 0 \\ 0 & \frac{1}{3} & 0 \\ 0 & \frac{1}{3} & 0 \end{pmatrix} \tag{2.23}$$

only for the pions 1 and n. However, (P12) guarantees insensitivity of our results to the choice of T_E at high multiplicity. We employ (2.15) at the end vertices for simplicity.

It is easy to generalize (2.21) to the two-pion spectrum for π^γ and π^δ:

$$\rho_N(y,\gamma;y',\delta) = \sum_{i\neq k} \overline{W}^n_{i,k}(y,y') Q^n_{i,k;\gamma,\delta}\,, \tag{2.24}$$

where for the case $i<k$

$$\overline{W}^n_{i,k}(y,y') = N_R \int_{-Y}^{0} dy_1 \int_0^Y dy_n F_{i-1}(|y_1 - y|) F_{k-i}(|y-y'|) F_{n-k}(|y'-y_n|)\,, \tag{2.25}$$

$$Q^n_{i,k;\gamma,\delta} = \sum_{\alpha,\beta,\xi,\eta} \frac{\langle 0|T^{i-1}|\beta\rangle\langle\beta|T_\gamma|\alpha\rangle\langle\alpha|T^{k-i}|\xi\rangle\langle\xi|T_\delta|\eta\rangle\langle\eta|T^{n-k}|0\rangle}{\langle 0|T^n|0\rangle}\,, \tag{2.26}$$

and $\overline{W}^n_{i,k}(y,y')$ is symmetric under the exchange of i,y and k,y' and $Q^n_{i,k;\gamma,\delta}$ is symmetric under the exchange of i,γ and k,δ.

We have the identity

$$\sum_{\gamma,\delta} \int \rho_N(y,\gamma;y',\delta)\,dy\,dy' = n(n-1)\,. \tag{2.27}$$

III. TWO-PARTICLE CORRELATIONS AT FIXED MULTIPLICITY

It is convenient to define the two-particle correlation function as

$$R_N(y,\gamma;y',\delta) = \frac{\rho_N(y,\gamma;y',\delta)}{\rho_N(y,\gamma)\rho_N(y',\delta)} - 1 \tag{3.1}$$

with (2.21) and (2.24), since the corresponding empirical quantity is not very sensitive to errors in normalization of experimental data.

Some remarks may be added on the connection between inclusive correlation function R and R_N. The inclusive single-particle distribution $\rho(y,\gamma)$ is given by

$$\rho(y,\gamma) = \sum_N \frac{\sigma_N}{\sigma_{\text{inel}}} \rho_N(y,\gamma)\,, \tag{3.2}$$

where σ_{inel} is the total inelastic cross section and σ_N the partial cross section at the multiplicity N. Similarly, we introduce the inclusive two-particle spectrum $\rho(y,\gamma;y',\delta)$. Then R is expressed in terms of R_N in the following manner:

$$R(y,\gamma;y',\delta) = \sum_N \frac{\sigma_N \rho_N(y,\gamma)\rho_N(y',\delta)}{\sigma_{\text{inel}}\rho(y,\gamma)\rho(y',\delta)} \times R_N(y,\gamma;y',\delta) + \left(\sum_N \frac{\sigma_N \rho_N(y,\gamma)\rho_N(y',\delta)}{\sigma_{\text{inel}}\rho(y,\gamma)\rho(y',\delta)} - 1\right). \tag{3.3}$$

Recall that N is the total multiplicity and not the charged multiplicity n_c. It seems reasonable to use the semi-inclusive quantities R_{n_c}, etc. in order to understand crudely the relation between R and R_N. Here we utilize the relation

$$N = \tfrac{3}{2}(n_c - 2) + 2\,, \tag{3.4}$$

assuming an equal weight for $\pi^\pm$ and π^0. In our model, (3.4) holds in an average sense. It is known empirically[43] that at 205 GeV/c R_{n_c} ($n_c = 4, 6$) receives a large positive contribution from diffraction dissociation. However, (P2) is affirmed again by reconstructing R from R_{n_c} through the use of (3.3): The contribution of low charge multiplicity is almost negligible.

Slansky[21] showed in a model calculation that the second kinematical term of the right-hand side of (3.3) gave almost the whole of the positive part of $R(0,\gamma;0,\delta)$. It is thus doubtful that the observed positivity[1] of $R(0,\gamma;0,\delta)$ is a direct result of intrinsic attraction between secondaries. It should be noted that both the second term and the coefficient R_N in (3.3) are symmetric around $(y,y') = (0,0)$ in the $y-y'$ plane. If an R_N shows an elongation along the line $y=y'$ in the contour map, so does R. The converse should be true, if N is larger than the mean multiplicity $\langle N\rangle$. Thus, the elongation is a crucial clue to the attraction.

Figure 2 illustrates the comparison between our calculated R_N with N given by (3.4) and R_{n_c} (Ref. 43) observed at 205 GeV/c.[44] One of the salient features is the peaks at $\Delta y \equiv y' - y = 0$ for both $y = 0$ and -1. That is, one would find an elongation along the line $y = y'$ in the contour map. It should be stressed that these attractive correlations have been obtained *without* having real clusters decaying into secondaries.

This apparent clustering is ascribed to the in-

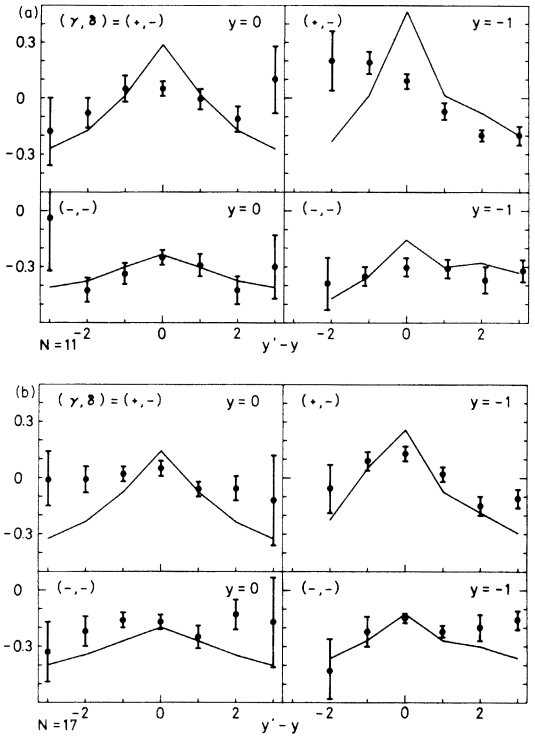

FIG. 2. (a) Two-particle correlations $R_{11}(y,\gamma;y',\delta)$ compared with empirical semi-inclusive correlations R_{n_c} ($n_c = 8$). They are calculated at the rapidities 0, ± 1, ± 2, and ± 3. The solid lines are drawn only as a guide. (b) Two-particle correlations $R_{17}(y,\gamma;y',\delta)$ compared with R_{n_c} ($n_c = 12$).

clusion of the kinematical region outside the strong-ordering limit. This is summed up by (2.12). Under strong ordering,

$$F_k(\Delta y) = \frac{D(D\Delta y)^{k-1}}{(k-1)!}\, e^{-D\Delta y}, \tag{3.5}$$

which vanishes at $\Delta y = 0$ for $k \geq 2$. That is to say, the next neighboring pions do not contribute to $F_k(0)$. Moreover, the probability function summed over k is flat. A similar situation occurs in DeTar's phase-space volume.[9] By contrast, $F_k(0) \neq 0$ for any k allowing for weak ordering, though it decreases with increasing k.

The negative-charge correlations $R_N(y,-;y',-)$ are in good agreement with the data. The apparent attraction arising from the weak ordering overcomes a repulsive tendency caused by the LCEX [(P9)]. On the other hand, $R_N(y,+;y',-)$ show steeper spikes than the empirical ones. A model with independent neutral clusters[4] yields better agreements with $R_{n_c}(y,+;y',-)$, but has repulsive correlations for pairs of negative pions, in disagreement with the data.

Energy-momentum-conservation constraints[21] improve our fits in the following points; first, R_N approaches zero at $|y|$, $|y'| = 3.0$. Secondly, the peaks at $\Delta y = 0$ and $y = -1$ are lowered.

The central values $R_N(0,\gamma;0,\delta)$ approach zero with increasing N. This trend is also suggested by experiment. Let us designate by $\langle k \rangle$ the representive number of links connecting the pions at y and y'. Probably, $\langle k \rangle$ increases with N. Then the distribution (2.12) will be flattened. Moreover, the mean number of particles per apparent cluster would slowly increase with energy, if indeed $\langle k \rangle$ increases with the average multiplicity.

IV. RAPIDITY-GAP DISTRIBUTION

Rapidity-spacing distributions have been measured for charged secondaries at high energies.[5,45,46] At relatively low energies, neutral particles have been detected in exclusive distributions.[47] It is a formidable task to study gaps between *charged* particles in our scheme. Throughout this section, our calculations concern gap lengths between adjacent pions, including both charged and neutral ones.

In Sec. IV A we shall study qualitatively the implication of weak ordering and LCEX. Our numerical evaluation will be presented in Sec. IV B.

A. Qualitative investigations

There is a simple and useful proposition for evaluating the contribution of a given graph. The rule is given as follows:

(R1) Suppose that two particles are separated by a gap length r and that j links (exchange objects) pass across the gap. It sould be noticed that these links have not necessarily immediate connections to the two particles. Then it follows from (P10) that the graph gives a gap distribution e^{-jDr}.

This ansatz is rather trivial. Recall that a graph occurs with the weight (2.7). Provided r is fixed, the length of the multiperipheral chain in rapidity cannot be reduced to be less than jr.

It follows from (R1) that a graph with strong ordering provides us with the distribution e^{-Dr} and that all graphs giving e^{-jDr} ($j \geq 2$) are not strongly ordered. For large r, only the former type, e^{-Dr}, survives.

The relation (2.2) implies[10] that the exchange picture with the Regge intercept $\alpha(0) \approx \frac{1}{2}$ is consistent with the data in the large-gap region, which indicate $D \approx 1$ there. Our model adopts this interpretation.

Before delving into the small-gap region, we may add some remarks on the distribution $P_{\Delta Q}(r)$ of rapidity gaps carrying specific charge ΔQ. If we order the rapidities of the n_c detected charged

particles $y^{(1)}<y^{(2)}<\cdots<y^{(n_c)}$, then the ith rapidity gap is said to carry charge

$$\Delta Q_i=\tfrac{1}{2}\Big[\sum_{k=i+1}^{n_c} Q(y^{(k)})-\sum_{k=1}^{i} Q(y^{(k)})\Big], \tag{4.1}$$

where $Q(y)$ is the charge of the particle outgoing at rapidity y.

The observed *shapes*[6] of $P_{\Delta Q}(r)$ for $\Delta Q=0$ and $|\Delta Q|=1$ are quite similar in the whole measured region. This observation rules out those models in which strictly neutral clusters are emitted independently in rapidity, as already remarked in Sec. III. On the other hand, our model would be consistent with the data, since charge exchanges $-1,0,+1$ occur with equal frequency. With the same reasoning, we expect

$$P_{\Delta Q=0}(r)\approx\tfrac{1}{2}P_{|\Delta Q|=1}(r). \tag{4.2}$$

The above relation is compatible with the experimental data.

Another empirical result is the absence of large gaps which carry more than one unit of charge. Such a truncation of the $|\Delta Q|>1$ distribution is realized in our model. We designate by $q_1\cdots q_j$ the charges carried by the j links and by ϵ_k the direction of the link carrying q_k; $\epsilon_k=1$ if the link points in the positive direction of rapidity, otherwise $\epsilon_k=-1$. It is clear that the total charge ΔQ exchanged across the gap is

$$\Delta Q=\sum_{k=1}^{j} q_k\epsilon_k. \tag{4.3}$$

Thus, the minimum number of links which pass across the gap specified by ΔQ is $|\Delta Q|$ (except for the case $\Delta Q=0$). We infer from (R1) that in the large-gap regime

$$P_{\Delta Q}(r)\sim\begin{cases}e^{-|\Delta Q|Dr} & (|\Delta Q|\geq 1),\\ e^{-Dr} & (\Delta Q=0).\end{cases} \tag{4.4}$$

This is an explicit expression for the truncation of the $|\Delta Q|>1$ distribution.

B. Numerical results

The measured distributions of rapidity spacings[5,46] deviate at small separations from a simple exponential behavior extrapolated from the large-gap regime. They show prominent spikes. Now we are in a position to attempt to reproduce this feature.

Our method is so complicated that we discuss it separately in the Appendix. The detailed behavior requires a knowledge of the technique. However, the physical meaning of the rise at small r in our model is summed up in proposition (R1). Indeed, a strongly ordered graph has the highest weight for any gap length. However, at small spacing, each of the other graphs makes an appreciable contribution to the rapidity-gap distribution $P(r)$, since e^{-jDr} $(j\geq 2)\sim 1$ in (R1). Furthermore, the number of configurations is large.

Figure 3 displays the rapidity-spacing distribution $P_N(r)$ at fixed multiplicity N at 205 GeV/c. The slope of $P_N(r)$ increases with N. This tendency is found in the experimental exclusive gap distributions.[47] The rate of increase in our model slows down for $N\gtrsim 11$. This may arise from omit-

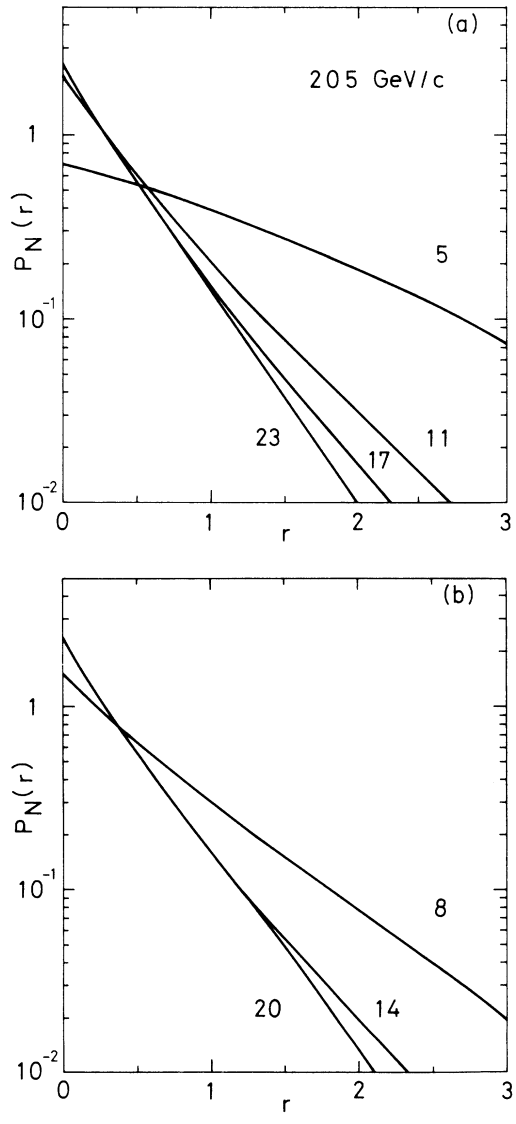

FIG. 3. (a) Distribution of gap lengths between adjacent particles in rapidity at fixed odd multiplicities. Gaps between a proton and a pion (end gaps) are excluded. Neutral particles are included. (b) Rapidity-gap distribution at fixed even multiplicities.

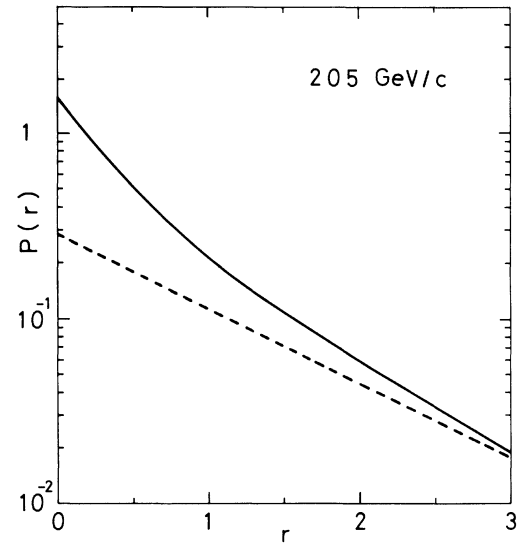

FIG. 4. Total rapidity spacing distribution shown with the solid curve. The dashed line represents $e^{(-Dr)}$ adjusted to the solid curve at $r=3.2$.

ting graphs which are dominant at high multiplicity (see the Appendix). It is clear from a model calculation in Ref. 22 that energy-momentum-conservation constraints raise the rate of the slope increase with N.

In Fig. 4 we depict the total distribution

$$P(r)=\sum_N \sigma_{n_c} P_N(r)/\sigma_{\text{inel}} \ , \tag{4.5}$$

using (3.4) for n_c and the empirical charge multiplicity distribution[36] for σ_{n_c}. A considerable spike is found at small r above the simple form e^{-Dr}. However, it is not sufficient to reproduce the observed distribution even[48] for charged tracks. [Interestingly, $P_{11}(r)$ gives a good fit to the latter.] Our hope is that the discrepancy will be filled up by consideration of all graphs and of energy-momentum-conservation constraints. Another kinematical constraint is the limitation of the total gap [see (4.1)],

$$\sum_{i=1}^{N-1} (y^{(i+1)}-y^{(i)}) \leq 2Y_\pi \ , \tag{4.6}$$

which is not taken into account here. The constraint (4.6) would lead to a steeper slope of $P(r)$.

V. CONCLUSIONS AND DISCUSSIONS

We have developed a statistical approach which allows a generalization of the strong-ordering hypothesis of the MPM. In the generalization, strong-ordered graphs have the highest probability in comparison with other graphs. It is suggested that the inclusion of some kinematical domain outside the strong-ordering limit and small-momentum transfer regions gives rise to a considerable part of the empirical attractive two-particle correlations and to the spike in the rapidity-gap distribution at small gaps. This extension of the kinematical region can be interpreted in an average sense as the inclusion of multiperipheral chains which are not always strongly ordered. In this picture, real clusters are not actually produced, but some of their effects are simulated by multiperipheral chains with weak ordering. This picture is physically based on the fact that the mean subenergy supplied to a link is relatively low (1–2 GeV).

In terms of Feynman graphs, our model corresponds to the ladder approximation. Twisted ladders, which appear as interference terms, might be an important correction to the ladder. However, in evaluating them, we must deal with the amplitudes and the phases would play an important role. It is uncertain whether or not the interference terms contribute without much cancellation among them to the quantities (a) and (b) in Sec. I, in the summation over all their configuration. We have neglected the contribution of the twisted ladders, assuming the cancellation.

Another possible approach to (a) and (b) is through Monte-Carlo simulations of the MPM.[49] So far the analysis has been limited to low-multiplicity phenomena and to inclusive processes with pion exchange.[1]

Let us explain in a little more detail than in Sec. II A how our picture is consistent with local compensation of charge. Compare the two cases: (a) three positive particles emitted successively in order of rapidity, and (ii) emission of two positive particles and a negative one. In a random-production picture (RPP), (i) and (ii) appear with equal frequency at large multiplicity ($n_c \geq 6$). The strong-ordering hypothesis (SOH) forbids (i). In our model, (i) occurs with a smaller weight as compared to (ii). The case (ii) receives the contribution of a graph with strong ordering as well as that of other graphs. Thereby we realize how many-track zones are suppressed. This simple example suggests that our model lies between the two extreme cases (RPP and SOH) with regard to local compensation of charge. A quantitative investigation will be interesting.

A two-channel MPM (Ref. 10) attributed the sharp rise of the rapidity-gap distribution to the lower trajectories (e.g., daughter trajectories). In this picture, the mean track number per zone $\langle n_z \rangle$ is still two, provided (P9) and strong ordering is assumed. This is inconsistent with the data (Table I).

Owing to the Pomeron exchange at the end links,

our model provides us with the same single-pion spectrum ρ_π for π^+ and π^-. Including neutron production will make ρ_{π^+} bigger than ρ_{π^-}.[18] Here the neutron spectrum is necessary as an input, since $D \neq 0$ in (2.1) and the distance between the pions 1 (or n) and the neutron should be explicitly considered.

Neglecting transverse-momentum dependence [(P5)] might prevent us from understanding attractive correlations between identical particles. Recent experiments[43,50] on azimuthal-angle correlations display a remarkable peak at zero angle. This might suggest that Bose-Einstein statistics play an essential role.[51] Further investigation is necessary.

There is still a controversy among experimentalists[3,52] about the neutrality of possible clusters. However, the distribution of rapidity gaps with specified charge transfer is the most direct evidence excluding the neutrality at present.

The clustering pictures may be classified into two categories[6]: (1) independent production of the clusters with rather flat rapidity distribution, and (2) exchange mechanism acting between the clusters. The independence in (1) may be only apparent and originate from a certain statistical average over all configurations of the cluster rapidities. The average number of clusters should be 5–6 even at CERN ISR energies[28] if particles per cluster are 3–4 (Ref. 53) in number[1,54] It is, therefore, doubtful whether such a statistical independence holds at currently available energies. The possibility of clusters emitted independently should correspond to a saturation of strong interactions.

On the other hand, the clusters of (2) would not be new objects reflecting some unexplored dynamical mechanism, but would be simply resonances.[7,18,24,26,55] It is interesting to note a similarity between (2) in the strong-ordering limit and our model in reproducing the local properties in rapidity. The resonancelike clustering means a small multiplicity of resonances as compared to the multiplicity of final particles.[18] Therefore, the kinematical domain is in the strong-ordering limit.[18] The decay spectrum corresponds to the size distribution (2.12) of the curled multiperipheral chain in rapidity space. Hence it will be difficult to discriminate between (2) and our picture.

ACKNOWLEDGMENTS

The authors would like to express sincere thanks to Professor E. Leader for careful reading of the manuscript and for enlightening discussions. He is very grateful to Professor Y. Yamaguchi, Dr. W. von Schlippe, Dr. T. Sasaki, and Dr. S. Yazuki for helpful discussions and critical comments. He is also thankful to the Theoretical Physics Division, Institute for Nuclear Study, University of Tokyo, and Department of Physics, Nagoya University (especially, Dr. K. Watanabe) for their hospitality. This work was performed under the financial support of the United Kingdom Science Research Council.

APPENDIX: METHOD FOR CALCULATING THE RAPIDITY-GAP DISTRIBUTION

1. Gap factors

Suppose that two particles are nearest neighbors in a multiperipheral chain. Then, the contribution of the graph to the distribution should be proportional to (2.1). We refer to such a contribution, which comes from a partial chain between the particles giving the gap, as a gap factor. For convenience of systematic calculations, we develop a graphical method. Equation (2.1) is shown by the graph (a) in Fig. 5.

In addition to (R1) in Sec. IV A, the rules for the graphs are given below:

(R2) A link is depicted by a solid line or curve.

(R3) The open circles represent pions produced at fixed rapidity points.

(R4) The black circles are pions whose rapidities are integrated over. If a black circle is to the left of an open one, we integrate the gap distribution over the former rapidity from the left kinematical boundary to the rapidity of the open circle. A similar rule is applied to a black circle to the right of an open one.

Throughout this appendix we make use of the assignment of pions in Sec. IV B. The graph 5(b) shows that the two pions l and m are next-nearest neighbors in the multiperipheral chain. The pion

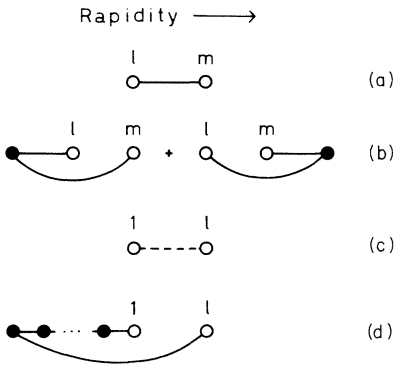

FIG. 5. Graphical representations of partial probability functions. (2.1), (A1), and (A4) correspond to (a), (b), and (c), respectively. The second term of (A4) is illustrated in (d).

between them in the chain is not allowed to enter the interval $[y_l, y_m]$, since $r = |y_l - y_m|$ is the gap length. The gap factor is

$$G_2(r) = \left(\int_{-Y}^{y_l} du + \int_{y_m}^{Y} du\right)\frac{D^2}{4} \times \exp(-D|y_l - u| - D|y_m - u|)$$
$$= \frac{D}{8} e^{-Dr}(\{1 - \exp[-D(Y + y_l)]\} + \{1 - \exp[-D(Y - y_m)]\}), \quad \text{(A1)}$$

where $u = y_{l+1}$. In the high-energy limit [(P3′)],

$$G_2(r) = \frac{D}{4} e^{-Dr}. \quad \text{(A2)}$$

Similarly, the gap factor of the next-to-next-nearest neighbor is

$$G_3(r) = \frac{D}{32}(5 + e^{-2Dr})e^{-Dr} \quad \text{(A3)}$$

under (P3′).

An examination of the calculation of (A2) and (A3) leads to the following rules:

(R5) A link passing through the gap carries the factor $\frac{1}{2}$, which represents the choice of its fixed direction between the two possible directions.

(R6) A black circle connected to two links in fixed opposite directions gives a factor $\frac{1}{2}$ in the high-energy limit [see the graph 5(b)].

Applying (R5) and (R6), one can obtain (A2), and (A3) and further higher gap factors $G_{m-l}(r)$. It is not difficult to see that $G_{m-l}(r)$ decreases with increasing $m - l$. We take account of them up to $|m - l| = 4$ in our calculations. Note that the gap factors are overestimated in (R6) near the kinematical boundary. However, we employ (R6) for simplicity.

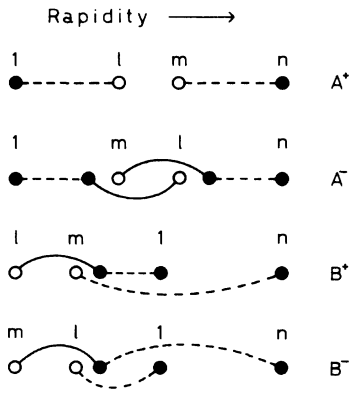

FIG. 6. Classification of multiperipheral chains giving a gap between the pions l and m. The B^+ and B^- class includes graphs which are symmetric with respect to the central rapidity to those shown here.

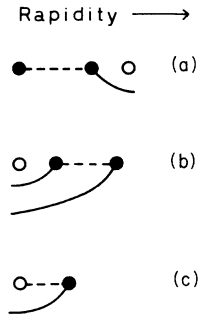

FIG. 7. Multiperipheral subchains as elements of end subchains. (a), (b), and (c) correspond to (A6), (A7) and (A8), respectiely.

2. End-subchain factors

Now we are in a position to evaluate the contribution of the partial chain including either the pions $1, \ldots, l$ or $m, \ldots, n$ to the rapidity-gap distribution. These partial probabilities will be referred to as end-subchain factors.

In the case that the left end subchain (the pions $1, \ldots, l$) does not pass the gap between the pions l and m, it is rather easy to estimate its contribution using the central-limit theorem.[38] Then the subchain is analogous to a trajectory of Brownian motion. For the initial distance $|y_l - y_1|$, the step $l - 1$ of first arrival at y_l is distributed with a density[41]

$$\frac{D|y_l - y_1|}{2[4\pi(l-1)^3]^{1/2}} \exp\left(-\frac{D^2|y_l - y_1|^2}{4(l-1)}\right)\theta(l-3) + C_{l-1}\exp(-D|y_l - y_1|), \quad \text{(A4)}$$

where $\theta(l - 3) = 1$ for $l \geq 3$, otherwise $\theta(l - 3) = 0$, and

$$C_k = \begin{cases} \frac{1}{2} & (k = 1), \\ (k-1)/2^{2k-1} & (k \geq 2). \end{cases} \quad \text{(A5)}$$

The second term of (A4) comes from the discrete nature in contrast to the continuous Brownian

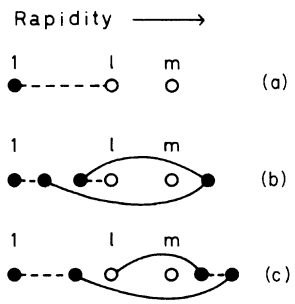

FIG. 8. Diagrams of the A^+ type which are considered in the present paper.

motion. This factor is shown by the graph 5(d). The whole term (A4) will be illustrated by a dashed line [Fig. 5(c)].

The gap is located either inside the interval $[y_1, y_n]$ or outside $[y_1, y_n]$. The two cases are referred to as the A and B class, respectively. Moreover, we have two possible cases: $y_l < y_m$ and $y_m < y_l$. These classes are shown by the superscript + and −, respectively. Thus we can divide all diagrams into 4 classes: A^+, A^-, B^+, and B^-. The simple graphs in these four classes are displayed in Fig. 6. A more general end subchain is a combination of the three kinds of subchain depicted in Fig. 7. For example, the end subchains of the A^+ class including one or two dashed lines [(A4)] are given in Fig. 8.

A systematic classification of an end subchain is given by the number of dashed lines.

We set $y = \min\{y_l, y_m\}$ and $z = \max\{y_l, y_m\}$. An explicit evaluation of the diagram 7(a) can be performed by integrating over the rapidities of the black circles: When $y < 0$,

$$H_a(y,k) = \frac{1}{(4\pi\lambda)^{1/2}}\{2\{1-\exp[-D(Y+y)]\} - (\pi\lambda)^{1/2} c^{\lambda}[\exp[-D(Y+y)]\{\operatorname{erfc}(-\sqrt{\lambda}) - \operatorname{erfc}(\tfrac{1}{2}D(Y+y)/\sqrt{\lambda} - \sqrt{\lambda})\} + \operatorname{erf}(\sqrt{\lambda} + \tfrac{1}{2}D(Y+y)/\sqrt{\lambda}) - \operatorname{erf}(\sqrt{\lambda})]\}\theta(\lambda-2) + C_{\lambda}(2\{1-\exp[-D(Y+y)]\} - D(Y+y)\exp[-D(Y+y)] - \tfrac{1}{2}\{1-\exp[-2D(Y+y)]\}), \tag{A6a}$$

where the right black circle is denoted by k and $\lambda = k-1$,

$$\operatorname{erf}(x) = \frac{2}{\sqrt{\pi}}\int_0^x e^{-t^2}dt, \quad \operatorname{erfc}(x) = 1 - \operatorname{erf}(x).$$

When $y > 0$,

$$H_a(y,\lambda) = \frac{e^{-Dy}}{(4\pi\lambda)^{1/2}}[2(1-e^{-DY}) - (\pi\lambda)^{1/2} e^{\lambda}\{e^{-DY}[\operatorname{erfc}(-\sqrt{\lambda}) - \operatorname{erfc}(\tfrac{1}{2}D(Y+y)/\sqrt{\lambda} - \sqrt{\lambda})] + [\operatorname{erf}(\tfrac{1}{2}DY/\sqrt{\lambda} + \sqrt{\lambda}) - \operatorname{erf}(\sqrt{\lambda})] - [\operatorname{erfc}(-\sqrt{\lambda}) - \operatorname{erfc}(\tfrac{1}{2}Dy/\sqrt{\lambda} - \sqrt{\lambda})]\}]\theta(\lambda-2) + C_{\lambda}e^{-Dy}[2(1-e^{-Dy}) - DYe^{-DY} + Dy(1-e^{-DY}) - \tfrac{1}{2}(1-e^{-2DY})]. \tag{A6b}$$

In diagram 7(b) the two black circles are supposed to be connected by μ links. Then, it is calculated as

$$H_b(z,\mu) = \frac{1}{(4\pi\mu)^{1/2}}\{1-\exp[-2D(Y-z)] - (\pi\mu)^{1/2}e^{\mu}[\operatorname{erf}(D(Y-z)/\sqrt{\mu} + \sqrt{\mu}) - \operatorname{erf}(\sqrt{\mu})] + (\pi\mu)^{1/2}e^{\mu}\int_0^{Y-z} dx\, e^{-2Dx}[\operatorname{erfc}(\sqrt{\mu} - \tfrac{1}{2}Dx/\sqrt{\mu}) - \operatorname{erfc}(\sqrt{\mu} + \tfrac{1}{2}D(Y-z-x)/\sqrt{\mu})]\}\theta(\mu-2) + \tfrac{1}{4}C_{\mu}\{1-\exp[-2D(Y-z)]\}. \tag{A7}$$

Graph 7(c) gives

$$H_c(z,\nu) = \frac{1}{(4\pi\nu)^{1/2}}\{1-\exp(\nu-\omega^2) - (\pi\nu)^{1/2}e^{\nu}[\operatorname{erfc}(\omega) - \operatorname{erf}(\sqrt{\nu})]\}\theta(\nu-2) + \tfrac{1}{2}C_{\nu}\{1-\exp[-2D(Y-z)]\}, \tag{A8}$$

where ν is the number of links between the white and black circles and $\omega = \sqrt{\nu} + \frac{1}{2}D(A-z)/\sqrt{\nu}$. An end subchain can be evaluated by applying rules (R1), (R5), and (R6), and by utilizing (A6), (A7), and (A8). For example, the diagram 8(b) has the following expression

$$(\tfrac{1}{2})^3 e^{-2Dr}\sum_{\lambda=1}^{l-4} H_a(y,\lambda)H_c(-y, l-\lambda-3). \tag{A9}$$

In the present paper, we take account of the end subchain graphs with one or two subchains denoted by the dashed line. From rule (R1) we can read off that only graph 6(a) gives the behavior e^{-Dr}. It follows from (R1), (R5), and (R6) that each contribution of other diagrams to $P_N(r)$ is smaller than that of this simplest one. However, they have many configurations in rapidity space. The number of the simplest graphs 6(a) is $n-1$, while

the two-dashed-line graphs of the A^+ type is

$$\sum_{k=1}^{n-2} k \sim O(n^2)$$

in number. When $n \gg 1$, the larger configuration compensates for their damping factor coming from (R5) and (R6) in the small-r region. This causes a spike to arise at small r. In the large-gap regime only the simplest graph remains dominant due to (R1).

---

*Present address: Department of General Education, Chukyo University, Yagoto-Motomachi, Showa-ku, Nagoya 466, Japan.

[1]I. M. Dremins and A. M. Dunaevskii, Phys. Rep. 18C, 159 (1975).

[2]A. Białas, in *Proceedings of the IV International Symposium on Multiparticle Hadrodynamics, Pavia, 1973*, edited by F. Duimio *et al.* (INFN, Pavia, 1974), p. 93; J. Ranft, in Proceedings of the Fifth International Symposium on Many-Particle Hadrodynamics, Eisennach-Leipzig, 1974 (unpublished); G. H. Thomas, in *Proceedings of the XVII International Conference on High Energy Physics, London, 1974*, edited by J. R. Smith (Rutherford Laboratory, Chilton, Didcot, Berkshire, England, 1974), p. I-83.

[3]C. Quigg, P. Pirilä, and G. H. Thomas, Phys. Rev. Lett. 34, 290 (1975).

[4]A. Guła, Lett. Nuovo Cimento 13, 432 (1975); Rutherford Laboratory Report No. RL-75-080 (unpublished).

[5]ANL–Fermilab–Stony Brook collaboration, unpublished work.

[6]P. Pirilä, G. H. Thomas, and C. Quigg, Phys. Rev. D 12, 92 (1975).

[7]D. Amati, A. Stanghellini and S. Fubini, Nuovo Cimento 26, 396 (1962); L. Bertocchi, S. Fubini, and M. Tonin, *ibid.* 25, 624 (1962); Chang Hong-Mo, J. Loskiewitz, and W. W. Allison, *ibid.* 57A, 93 (1968).

[8]G. F. Chew and A. Pignotti, Phys. Rev. 176, 2112 (1968).

[9]C. E. DeTar, Phys. Rev. D 3, 128 (1971).

[10]D. R. Snider, Phys. Rev. D 11, 140 (1975).

[11]There is a controversy about the existence of the attractive semiinclusive correlations (Ref. 12). However, according to discussions in Sec. IV, the obvious attractive *inclusive* correlations lead to attractive correlations at fixed multiplicity.

[12]J. Erwin *et al.* (Davis-Berkeley collaboration), Phys. Rev. Lett. 33, 1443 (1974); S. R. Amendolia *et al.* (Pisa–Stony Brook collaboration), Phys. Lett. 48B, 359 (1974); H. Dibon *et al.*, Phys. Lett. 44B, 313 (1974).

[13]F. Zachariasen and G. Zweig, Phys. Rev. 160, 1322 (1967).

[14]C. Bromberg *et al.* (Rochester-Michigan collaboration), Phys. Rev. D 12, 1224 (1975); H. Blumenfeld *et al.* (French-Soviet collaboration), Serpukhov Report No. M-12 (unpublished).

[15]A. Kryzywicki and D. Weingarten, Phys. Lett. 50B, 265 (1974); D. Weingarten, Rochester Report No. UR-505 (unpublished); A. Krzywicki, in *Proceedings of the X Rencontre de Moriond*, Meribel-les-Allues, 1975, edited by J. Tran Thanh Van (Université de Paris–Sud, Orsay, 1975), Vol. I.

[16]A. Kryzywicki, C. Quigg, and G. H. Thomas, Phys. Lett. 57B, 369 (1975).

[17]Without (1), assumption (2) leads to attractive correlations between positive and negative particles (T. Sasaki, private communication). The model is described in Ref. 18. However, it gives repulsive or vanishing correlations for either positive or negative pairs of secondaries.

[18]N. Murai and T. Sasaki, Phys. Rev. D 11, 1083 (1975).

[19]E. L. Berger, Nucl. Phys. B85, 61 (1975).

[20]Z. Koba, H. B. Nielsen, and P. Olesen, Nucl. Phys. B40, 317 (1972); P. Olesen, in *Proceedings of the IV International Symposium on Multiparticle Hadrodynamics, Pavia, 1973* (Ref. 2), p. 463.

[21]R. Slansky, Nucl. Phys. B73, 477 (1974).

[22]N. Murai, Phys. Lett. 56B, 315 (1975).

[23]T. Ludlam and R. Slansky, Phys. Rev. D 12, 59 (1975); 12, 65 (1975).

[24]N. Murai and T. Sasaki, Prog. Theor. Phys. 54, 154 (1975).

[25]A. Basetto, M. Toller, and L. Sertorio, Nucl. Phys. B34, 1 (1971); L. Brink, W. N. Cottingham, and S. Nussinov, Phys. Lett. 37B, 192 (1971); N. Murai and K. K. Phua, Lett. Nuovo Cimento 5, 575 (1972); T. Sasaki and N. Murai, Phys. Rev. D 9, 3070 (1974); Prog. Theor. Phys. 50, 610 (1973); T. Sasaki, thesis, Univ. of Tokyo, 1973 (unpublished); J. Randa, Phys. Rev. D 11, 3232 (1975); F. Hayot, Lett. Nuovo Cimento 12, 676 (1975).

[26]K. Böckmann, Rapporteur's talk at the International Conference on High Energy Physics, Palermo, 1975 (unpublished); F. C. Winkelmann *et al.* (LBL–Fermilab collaboration), Phys. Lett. 56B, 101 (1975).

[27]R. F. Amann and P. M. Shah, Phys. Lett. 42B, 353 (1972).

[28]H. Bøggild, in *Proceedings of the III International Colloquium on Multiparticle Reactions, Zakopane, Poland, 1972* (Institute for Nuclear Research, Warsaw, 1972).

[29]M. L. Mehta, *Random Matrices* (Academic, New York, 1967).

[30]V. Barger, in *Proceedings of the XVII International Conference on High Energy Physics* (Ref. 2), p. I-193.

[31]*Higher Transcendental Functions* (Bateman Manuscript Project), edited by A. Erdelyi (McGraw-Hill, New York, 1953), Vol. II.

[32]W. R. Frazer, L. Ingber, C. H. Mehta, C. H. Poon, D. Silverman, K. Stowe, P. D. Tin, and H. J. Yesian, Rev. Mod. Phys. 44, 284 (1972).

[33]C. J. Hamer, Phys. Rev. D 7, 2723 (1973); C. J. Hamer and R. F. Peierls, Phys. Rev. D 8, 1358 (1973).

[34]Duality is applied to only imaginary part of amplitudes. Resonances occur as peaks over the form (2.1).

[35]This estimation does not appreciably depend on energy, if $\langle n_c \rangle \sim \ln s$.

[36]G. Charlton *et al.* (ANL–Fermilab–Iowa-Michigan-Maryland collaboration), Phys. Rev. Lett. 29, 515 (1972).

[37]We deal with one-dimensional (rapidity) space. Therefore, backward exchange between identical particles gives the same type of graph as the forward exchange.

The former is excluded by statistics.
[38]A. I. Khinchin, *Mathematical Foundations of Statistical Mechanics* (translated from Russian by G. Gamov) (Dover, New York, 1949).
[39]J. I. Kemeny and J. L. Shell, *Finite Markov Chains* (D. Van Nostrand, New York, 1960).
[40]W. Burdett *et al.* (Nashville-BNL collaboration), Nucl. Phys. B48, 13 (1972).
[41]E. B. Dynkin and A. A. Yushkevich, *Markov Processes* (translated from Russian by J. S. Wood) (Plenum, New York, 1969).
[42]It took about 30 sec to calculate the two-particle correlation for each N. The entire calculation of rapidity spacing distribution took 6.5 min. on an IBM 370.
[43]R. Singer *et al.* (ANL–Fermilab–Stony Brook collaboration), Phys. Lett. 49B, 481 (1974).
[44]Unfortunately, we cannot modify R_N to compare it with the data in Ref. 45. The final state does not have definite charge multiplicity in our model.
[45]Michigan-Argonne-Fermilab-Iowa-Maryland collaboration, Phys. Lett. B (to be published).
[46]Michigan-Rochester collaboration (unpublished).
[47]M. Barrier *et al.* (LPNHE-Pavia-Durham-Bari collaboration), Nuovo Cimento 26A, 259 (1975).
[48]Picking up charged tracks flattens the slope of $P(r)$. See Ref. 22.
[49]K. G. Boreskov *et al.*, Yad. Fiz. 15, 361 (1972) [Sov. J. Nucl. Phys. 15, 203 (1972)]; *ibid.*, 15, 557 (1972) [15, 309 (1972)].
[50]K. Eggert *et al.* [Aachen-CERN-Heidelberg-München (MPI) collaboration], Nucl. Phys. B86, 201 (1975); C. M. Bromberg *et al.*, Phys. Rev. D 9, 1864 (1974); T. Ferbel, in Proceedings of the Fifth International Symposium on Many-Particle Hadrodynamics, Eisennach-Leipzig, 1974 (unpublished); M. Sabau, in Proceedings of the Fifth International Symposium on Many-Particle Hadrodynamics, Eisennach-Leipzig, 1974 (unpublished).
[51]M. Biyajima and O. Miyamura, Phys. Lett. 53B, 181 (1974); 57B, 376 (1975); G. Ranft and J. Ranft, *ibid.* 53B, 188 (1974); 57B, 373 (1975); Nucl. Phys. B86, 63 (1975); B92, 207 (1975); J. Steinhoff, *ibid.* B55, 132 (1973); L. Matssor, Phys. Rev. D 10, 2663 (1974); A. Arneodo and G. Plaut, Nucl. Phys. B97, 51 (1975).
[52]V. Blobel *et al.* [Bonn-Hamburg-München (MPI) collaboration], Nucl. Phys. B88, 18 (1975).
[53]This value is obtained in the analyses of two-particle correlations. Reference 3 and the paper by L. I. Perlovsky [Phys. Lett. 56B, 45 (1975)] suggest different values in studying the rapidity-gap distribution and repulsive interaction between clusters, respectively.
[54]P. Pirilä and S. Pokorski, Phys. Lett. 43B, 502 (1973); E. L. Berger and G. C. Fox, Phys. Lett. 47B, 162 (1973); F. Hayot and A. Morel, Nucl. Phys. B68, 323 (1974); B68, 312 (1974); W. Schmidt-Parzefall, Phys. Lett. 46B, 399 (1973); M. Le Bellac, H. I. Miettinen, and R. G. Roberts, *ibid.* 48B, 115 (1974).
[55]References cited by C. J. Hamer, Phys. Rev. D 10, 1458 (1974).